STUDENTSKÁ PŘEHLÍDKA

Students 1 - Monday, June 18

S1

FOX GRID – MULTI PC EXECUTION ACCELERATED VERSION OF THE FOX SOFTWARE FOR POWDER DATA STRUCTURE SOLUTION

J. Rohlíček, M. Hušák

Department of Solid State Chemistry, Institute of Chemical Technology, Prague,Technická 5, 166 28 Prague 6, Czech Republic
rohlicej@vscht.cz

There exist a number of sophisticated and really fast methods for structure determination from powder diffraction data, but there are still a lot of situations for which non-sufficient computational power is the bottleneck. Typical examples of computational heavy situations: multiple fragments in the asymmetric unit cell, preferred orientation, flexible fragment. We had tried to solve the performance problem by modifying the FOX [1] structure solution code for an automatic multi PC parallel run.
See page 83 for more.

S2

EXPANDING FOX FOR MICROSTRUCTURE ANALYSIS

Z. Matěj*, L. Nichtová, R. Kužel

Department of Condensed Matter Physics, Faculty of Mathematics and Physics, Charles University, Ke Karlovu 5, 121 16 Praha 2, Czech Republic
e-mail: matej@karlov.mff.cuni.cz*

Program FOX for structure solution from powder diffraction was extended by routines for x-ray microstructure analysis of small-grain or defect materials, thin films, or strained and textured samples in different diffraction geometries. General interface for convolution of various profile broadening models was created. It is possible to handle both physically relevant as same as phenomenological broadening models. Second part of extensions involves intensity corrections for texture and absorption in layered samples. General texture calculator can be used for other purposes such as pole figure simulation. Program was applied to strongly deformed metal (Cu) samples and to nanocrystalline TiO_2 powders and thin films.

Extended contribution submitted for publication in Materials Structure, no. 3.

S3

PAINTING COPPER-BASED PIGMENTS, THEIR CHEMISM AND DEGRADATION

S. Švarcová[1], J. Schweigstillová[2], E. Kotulanová[1], P. Bezdička[1]

[1]Institute of Inorganic Chemistry AS CR, v.v.i., ALMA laboratory, 250 68 Husinec-Řež, Czech Republic
[2]Institute of Rock Structure and Mechanics AS CR, v.v.i., V Holešovičkách 41, 182 09 Praha 8, Czech Republic
svarcova@iic.cas.cz

The art objects with porous nature, such as wall paintings or sandstone statues, are often exposed to attack of salts present in surrounding environment which results in deterioration of these art works. Crystallizing salts may be locally concentrated as efflorescence on the art work surface or as invisible subflorescence in the subsurface bulk of the porous materials that causes mechanical damages of artworks. Additionally, the presence of salts can also lead to the decay or alteration of pigments accompanied by a change of the original colour [1, 2].

Because of their sensitivity to moisture and air pollution, some pigments were not recommended for using in wall paintings. However, we commonly find some of them in real samples. Salts of copper widely used as relatively cheap blue and green pigments are very good example. Many copper-based pigments are basic salts that are

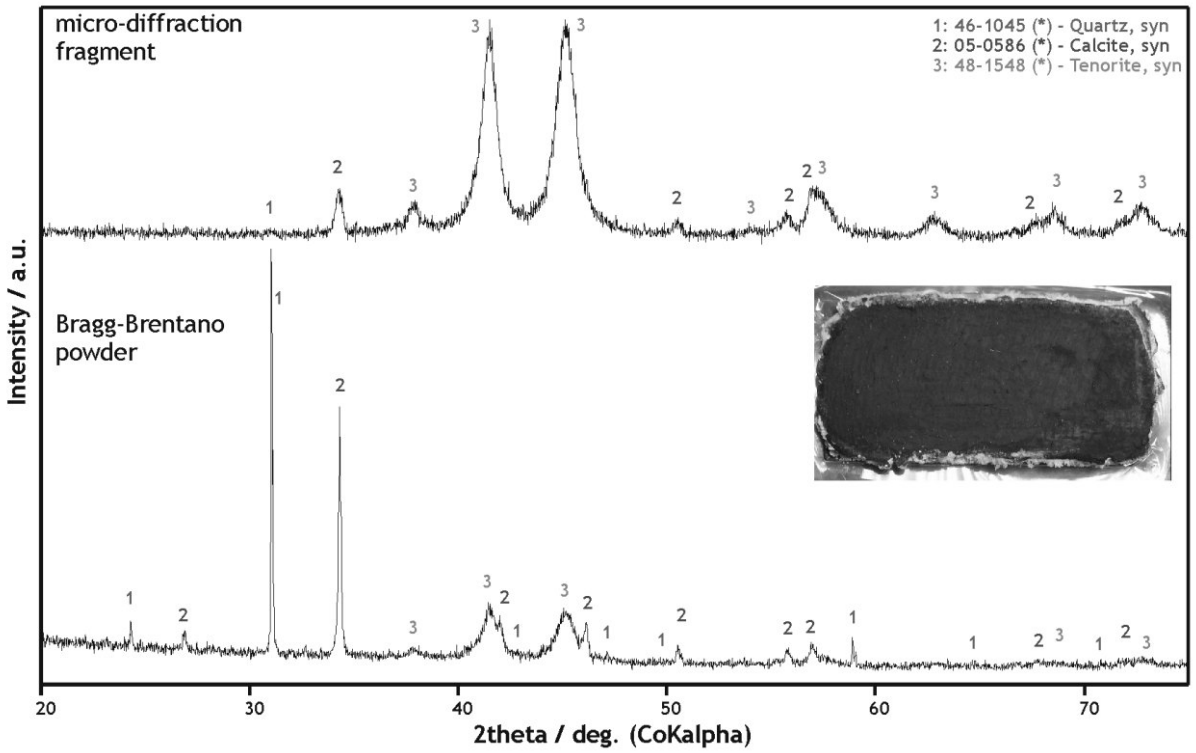

Figure 1. The comparison of diffractograms measured in Bragg-Brentano and microdiffraction geometry on the corroded malachite model layer.

metastable if the activity of other ions changes during wetting the colour layer by salt solution. Conversion to further salt can change the pigment colour, but even this fact cannot be easily revealed by examination of the artwork in its present state. One of the reasons is that it is not always possible to distinguish original phases and the products of their salt attack. Malachite, as well as basic copper chlorides, atacamite and paratacamite, are sometimes supposed to be the degradation products of mineral pigment azurite [3]. On the other hand, malachite, atacamite and paratacamite were reported also as used pigments [4].

We have investigated the composition of real samples as well as we have performed several types of model experiments in order to study the possible interaction between selected pigments and salt solutions. Chosen salts either occur in the environment (e.g. Na_2SO_4, $CaSO_4$, NaCl, $NaNO_3$, $Ca(NO_3)_2$, urea) or their presence in an art work is a result of some restorer action (e.g. Chelatone III, $NaHCO_3$, $(NH_4Cl)_2CO_3$) In the first type of experiments we mixed selected copper-based pigments, i.e. azurite, malachite and neutral verdigris, with a range of salt solutions and left them to react for ca two months. The reaction products were analyzed using powder XRD. Simultaneously we painted azurite and malachite on the surface of building bricks experimental bodies covered by trilaminar plaster prepared according the historical recipes. We used both historical techniques for painting, "secco" on dry plaster and "genuine fresco" on wet plaster. In the case of "secco" technique we exposed experimental bodies to selected solutions that evaporated through the porous body affecting finally the colour layer. Colour changes were monitored and products of alterations were measured as powder using powder X-ray diffraction in Bragg-Brentano geometry and as fragment of colour layer using powder X-ray micro-diffraction. In the case of "fresco" the both painted surfaces got grey till the following day, thus we did not perform further experiments.

Powder X-ray micro-diffraction could significantly enhance the detection of minor phases, as demonstrated in Fig. 1. In this case the experimental body was painted by malachite and exposed to the solution of $NaHCO_3$, which resulted in complete blackening of the originally green surface. When the powdered sample, scraped from the surface, was measured using conventional XRD expected tenorite (CuO) could be only poorly identified, whereas when the fragment of surface layer was measured using powder XRD micro-diffraction the presence of tenorite was more apparent.

1. S.G. Schirripa & D. Paoletti, *J. optics-nouvelle revue d optique*, **70**, (1996), 133.
2. B. Salvadori, V. Errico, M. Mauro, E. Melnik, L. Dei, *Spectroscopy letters*., **36**, (2003), 501.
3. L. Dei, A. Ahle, P. Baglioni, D. Dini, E. Ferroni, *Studies in Conservation*, **43**, (1998a), 80.
4. D. Scott, *Studies in Conservation*, **45**, (2000), 39.

Acknowledgements

The authors appreciate the Grant Agency of AS CR for the financial support of the project No. B400320602.

S4

COMPARISON OF RESULTS OF THE MICRODIFFRACTION AND MACRODIFFRACTION OF FORENSIC SAMPLES MEASUREMENTS

I. Jebavá[1], V. Goliáš[1], M. Kotrlý[2]

[1]Univerzita Karlova v Praze, Přírodovědecká fakulta, Ústav geochemie, mineralogie a nerostných zdrojů, Albertov 6, 128 43, Praha 2
[2]Kriminalistický ústav Praha PČR, Bartolomějská 10, 110 00, Praha 1
E-mail: Iva.Jebava@seznam.cz

The aim of this work was comparison of microdiffraction and classic Bragg-Brentano ("macrodiffraction") instrumentation of identical small-volume samples. The alumina (corundum, SRM 676) standard and five real forensic samples of unknown composition was studied using X´Pert PRO (PANalytical) difractometer system. Standard and all of the samples suggest better angle resolution (FWHM) in Bragg-Brentano geometry than in microdiffraction. In case of real forensic samples was the microdiffraction more suitable, because it manage to identify more crystallic phases, however at the price of time-consuming delay.

Extended contribution submitted for publication in Materials Structure, no. 3.

S5

CONTRIBUTION TO THE CRYSTALLOGRAPHY OF Bi CHALCOGENIDES

R. Pažout[1], M. Dušek[2]

[1]Institute of Chemical Technology, Technická 5, Praha 6,166 28, Czech Republic
[2]Institute of Physics, Na Slovance 2, 182 21 Praha 8, Czech Republic
richard.pazout@vscht.cz

Synthetic and natural chalcogenides are studied as perspective electrical materials with interesting semi-conductive properties. Structure of natural phase $AgPbSbBi_2S_6$, known as the mineral gustavite, has been solved and refined to R value of 4.19. The crystal structure of double-substituted gustavite was determined on a sample from hydrothermal veins of the Kutná Hora polymetallic deposit extracted from polished section pre-analysed on electron microprobe with WDS detection in order to ensure exact and single-phase composition. Two kinds of substitution are present in the sample: $Ag^+ + Bi^{3+}$ 2 Pb^{2+} and Bi^{3+} Sb^{3+}. The data were collected on X-ray single crystal diffractometer Xcalibur (Oxford Diffraction) with MoKá radiation and CCD detector Sapphire 2. The indexation and data reduction was carried out using program Chrysalis. In order to enable reliable refinement of crystal shape a highly redundant data set was measured with average redundancy 7.6. Absorption correction of the strongly absorbing sample (= 54 mm^{-1}) was then carried out using a combination of tools: refinement of face distances using program Crysalis, refinement of face distances and angles with program X-Shape and - finally - combination of the shape and multi-scan absorption correction. Initial positional parameters were obtained by charge flipping method using the program Superflip [1], the refinement was carried out in the program Jana2006 [2]. In the first stage the substructure (characterized by strong to medium-strong reflections in the reciprocal lattice) was refined in the space group Cmcm. The refined atomic positions and displacement parameters were used as a starting point for the refinement of the superstructure (characterized by weak to very weak reflections in the reciprocal lattice) in the space group $P2_1/c$. In the final stages of refinement 58 parameters were refined including occupancies using 1386 independent reflections, yielding R factors R_{obs} = 4.19 for 366 nonequivalent observed reflections with I 3 , R_{wobs} = 3.39, $R_{(all)}$ = 23.62, $R_{w(all)}$ = 4.40, GOF_{obs} = 1.77, $GOF_{(all)}$ = 1.11. Bond valence analysis carried out using the program Ivton [3] confirmed that the atom with bicapped trigonal coordination is Pb, all other sites being mixed and octahedrally coordinated.

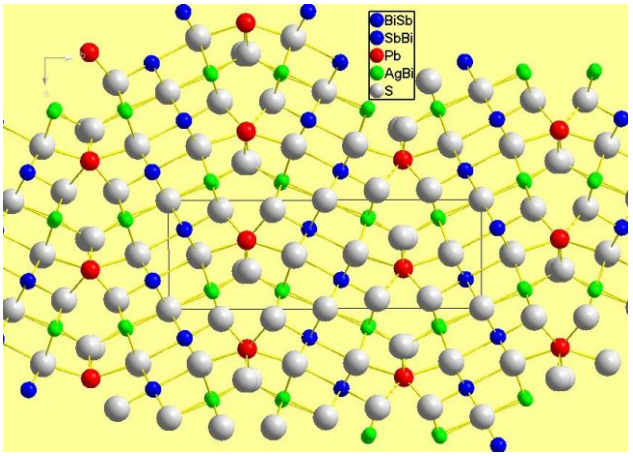

Figure 1: Crystal structure of natural $AgPbSbBi_2S_6$

Natural $AgPbSbBi_2S_6$ is known as the mineral gustavite of the lillianite homologous series with the composition $^{4.02}Gus_{107.7}$, Bi/(Bi+Sb) = 0.69, space group $P2_1/c$, a = 7.04 b = 19.436 c = 8.335 Å, = 107.12, Z = 4. The crystal

structure of gustavite has five cation sites: one Pb site, two mixed Bi/Sb sites, two mixed Bi/Ag sites and seven sulphur positions. The structure is presented in Fig. 1. It consists of layers of PbS-like (NaCl) slabs running diagonally formed by four octahedra separated by a layer of Pb atoms in trigonal primatic coordination on the plane of unit cell twinning Trigonal prismatic site is fully occupied by Pb, the Bi-Sb and Ag-Bi substitutions occur in the octahedral sites in the central and marginal portion of the slabs, respectively.

1. L. Palatinus, *Program Superflip*, http://superspace.epfl.ch/superflip/, 2007
2. V Petříček, M. Dušek, L. Palatinus, *JANA2006,. The crystallographic computing system*. Institute of Physics, Czech Republic, 2006.
3. T. Balić-Žunić, I. Vicković, *IVTON, a program for the calculation of geometrical aspects of crystal structures and some crystal chemical applications. Geological Institute, University of Copenhagen, Denmark, 1994.*

Students 2 - Tuesday, June 19

S6

GLYCOSYLATION OF IGG-FC

P. Kolenko[1,2], J. Dohnálek[1], J. Dušková[1], T. Skálová[1], J. Hašek[1]

[1]Institute of Macromolecular Chemistry AS CR, v.v.i., Heyrovského nám.2, 162 00, Prague 6
[2]Dept.of Solid State Physics, FJFI, CTU, Trojanova 13, 120 00, Prague 2, kolenko@imc.cas.cz

The crystallisable fragment (Fc) of antibody (Ig) mediates the response of the adaptive part of immune system. Ten structures of IgG-Fc in non-liganded form were deposited in the Protein Data Bank [1] up to now. Although chemical properties and the structure of Fc were assessed by many physical and chemical techniques, some new details of the oligosaccharide structure were known after evaluation of the most recently deposited structure [2] and our non-deposited structure [3].

Localization of fucose

Interpretation of saccharides in electron density maps is difficult. Inspection of structures and electron density maps showed doubtful structure refinement of fucose. All structures of Fc deposited by December 2006 contained beta-L-fucose. Low-resolution structural data did not allow distinguishing the proper glycoform, e.g. two of the structures with electron density maps are shown in Fig. 1.

In May 2007, the structure of non-liganded IgG1-Fc with the highest resolution of 2 Å [2] was deposited in the PDB. Our structure solution of IgG2b-Fc was described two years ago [3]. The structure contains alpha-L-fucose. The experimental data (high resolution limit lower than 2.2 Å) allowed localization of fucose with good agreement with electron density (Fig.2).

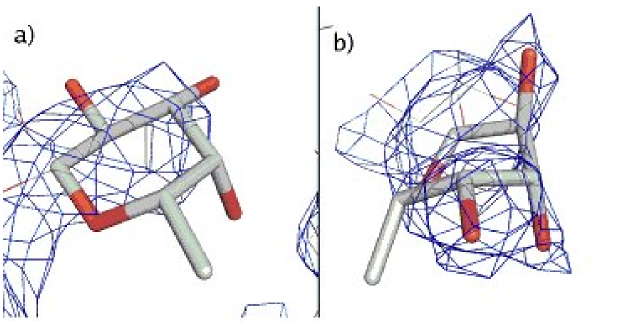

Figure 1. Electron density map in surroundings of fucose for structures: a) 1I1C, b) 1H3U. The figures were prepared with Pymol [4].

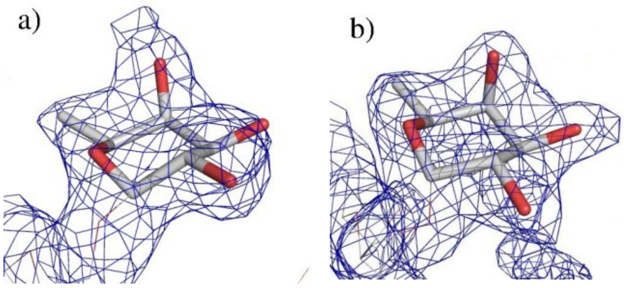

Figure 2. Electron density map in surroundings of fucose for structures: a) 2DTQ, b) our structure. The electron density observed in the lower left corner belongs to the continuation of the oligosaccharide chains in both cases.

About 30 % of all PDB entries containing saccharides have at least one error in glycan interpretation [5]. The glycosylation and quality of structures deposited in the PDB will be discussed.

1. H.M. Berman, J. Westbrook, Z. Feng, G. Gililand, T.N. Bhat, H. Weissing, I.N. Shindyalov, P.E. Bourne, *Nucleic Acids Research*, **28**, 2000, 235-242.
2. S. Matsumiya, Y. Yamaguchi, J. Saito, M. Nagano, H. Sasakawa, S. Otaki, M. Satoh, K. Shitara, K. Kato, *Journal of Molecular Biology*, **368**, 2007, 767.
3. P. Kolenko, J. Dohnálek, R. Š ouračová, T. Skálová, G. Tiščenko, J. Dušková, J. Hašek, *Materials Structure*, **12**, 2005, 146.
4. W.L. DeLano, *The PYMOL User's Manual*, DeLano Scientific, San Carlos, CA, USA, 2002.
5. T. Lütteke, M. Frank, C-W. von der Lieth, *Carbohydrate Research*, **339** [illegible]

The project is supported by the Ministry of Education, Youth and Sports of the Czech Republic (project no. 1K05008) and by the project "Spine 2 – Complexes" of the European Commission (LSHG-CT-2006-031220).

S7

THE INFLUENCE OF I47A MUTATION ON REDUCED SUSCEPTIBILITY TO THE PROTEASE INHIBITOR LOPINAVIR

Klára Šašková[1,2], Milan Kožíšek[1,2] , Jiří Brynda[1,4], Martin Lepšík[1], Ladislav Machala[3] and Jan Konvalinka[1,2*]

[1]Institute of Organic Chemistry and Biochemistry, Academy of Sciences of the Czech Republic, Flemingovo n. 2, 16610 Praha 6, Czech Republic
[2]Dep. of Biochemistry, School of Science, Charles University, Hlavova 8, 128 43 Praha 2, Czech Republic
[3]AIDS Center at the Clinic of Infectious Diseases, Faculty Clinic Bulovka, Budinova 2, CZ- 12000 Praha 8, Czech Republic
[4] Institute of Molecular Genetics, Academy of Science of the Czech Republic, Flemingovo n.2, 166 10 Praha 6, Czech Republic
**corresponding author, E-mail: konval@uochb.cas.cz, fax: +420 220 183 578*

The introduction of protease inhibitors (PI) in mid 90´s led to decreased mortality and prolonged life expectancy of HIV-positive patients. However, the selection pressure of a virostatic leads to rapid selection of viral variants resistant towards a specific inhibitor. Different PIs select different patterns of mutations. Lopinavir (LPV) is a second generation PI that was rationally designed to inhibit resistnant PR species. Its resistance profile has not been clearly defined yet. Mutations at 11 amino acid positions in protease (PR) coding region were identified as associated with reduced susceptibility (lopinavir mutation score). The higher number of mutations accumulated at these positions, the bigger the resistance to LPV. However, individual mutations resulting in LPV resistance are very rare. Recently, mutation I47A has been identified to confer high–level resistance.

In this work, we set to identify the relative contributions of I47A mutation and others from the lopinavir mutation score. We designed a panel of resistant PR species containing I47A substitution in the backround of the wild–type PR and also in the backround of a highly resistant specimen from a patient. Individual recombinant PRs were expressed, purified and characterized and their inhibition profiles were analysed with a panel of PIs. The X-ray analysis of the protease containing I47A mutation in complex of LPV showed the loss of van der Waals interactions of Ala47 with lopinavir phenoxyacetyl moiety. Futhermore, energy calculations confirmed weaker affinity of LPV and the decrease of both electrostatic and van der Waals interactions.

S8

CRYSTALLOGRAPHIC STUDY OF *ESCHERICHIA COLI* FLAVOPROTEIN WRBA, A NEW NAD(P)H-DEPENDENT QUINONE OXIDOREDUCTASE

J. Wolfová[1,2], J. Brynda[1,3], J. R. Mesters[4], J. Carey[5], R. Grandori[6], I. Kutá Smatanová[1,2]

[1]Institute of Physical Biology, University of South Bohemia České Budějovice, Zámek 136, CZ-373 33 Nové Hrady, Czech Republic
[2]Institute of Systems Biology and Ecology, Academy of Science of the Czech Republic, Zámek 136,CZ-373 33 Nové Hrady, Czech Republic
[3]Institute of Molecular Genetics, Academy of Sciences of the Czech Republic, Flemingovo nám. 2, CZ-16637 Prague 6, Czech Republic
[4]Institute of Biochemistry, Center for Structural and Cell Biology in Medicine, University of Lübeck, Ratzeburger Allee 160, 23538 Lübeck, Germany
[5]Chemistry Dep., Princeton University, Washington Rd and William St, Princeton, NJ 08544-1009, USA
[6]Dep. of Biotechnology and Biosciences, Univ.of Milano-Bicocca, Piazza della Scienza 2, 20126 Milan, Italy
julinka.w@tiscali.cz

The flavoprotein WrbA from *Escherichia coli* represents a new family of multimeric flavodoxin-like proteins implicated in cell protection against oxidative stress. The recently revealed NAD(P)H-dependent quinone oxidoreductase activity stimulated determination of crystal structures of *E. coli* WrbA and the following search for structural features characterising the new family of redox active proteins.

Well-formed tetragonal crystals of WrbA protein in complex with its cofactor flavin mononucleotide (FMN) were obtained using standard vapor-diffusion techniques. The diffracion data were collected for two different crystal forms and the X-ray crystal structures have been determined to a resolution of 2.0 Å and 2.6 Å.

Lower crystallizability observed previously for *E. coli* WrbA apoprotein (without bound FMN) indicates the posi-

tive influence of FMN on crystallization of WrbA protein. The suggested effect for FMN in favouring crystal lattice formation through the specific interaction with protein motivated further search for better crystals of WrbA apoprotein. Based on crystallization conditions found for WrbA-FMN complex the diffraction-quality crystals of WrbA apoprotein were obtained. Dependence of apoprotein crystal growth on temperature was observed. The crystals diffracted up to a resolution of 1.85 Å.

This work is supported by the Ministry of Education of the Czech Republic (projects: Kontakt ME640, MSM6007665808, LC06010) and by the Academy of Sciences of the Czech Republic (AV0Z60870520). We are grateful to the staff of EMBL/DESY in Hamburg for the support during data collection. Diffraction measurements at the synchrotron DESY/EMBL were supported of the European Community, Research Infrastructure Action under the FP6 "Structuring the European Research Area Specific Programme" to the EMBL Hamburg Outstation, Contract Number RII3-CT-2004-506008.

Extended contribution submitted for publication in Materials Structure, no. 3.

S9

STRUCTURAL AND FUNCTIONAL STUDIES OF HIGHER PLANTS PHOTOSYSTEM II

Tatyana Prudnikova[1], Michal Kutý[1,2], José A. Gavira[3], Peter Palenčár[1], František Vácha[1,5], Pavlína Řezáčová[4], Juan M. García-Ruiz[3] and Ivana Kutá Smatanová[1,2]

[1]Institute of Physical Biology USB CB, Zamek 136, 373 33 Nove Hrady, Czech Republic
[2]Institute of Systems Biology and Ecology AS CR Zamek 136, 373 33 Nove Hrady, Czech Republic
[3]Laboratorio de Estudios Cristalografico, Edf. Lopez Neira, P.T. Ciencias de la Salud, Avenida del Conocimiento, s/n, 18100 Armilla, Granada, Spain
[4]Institute of Molecular Genetics AS CR, Flemingovo n. 2, 16637 Prague, Czech Republic, current address: Dep. Biochemistry, UT Southwestern Medical Center, 5323 Harry Hines Boulevard, Dallas, Texas 75390-8816
[5]Biological Centre IPMB AS CR, Branisovska 31, 370 05 Ceske Budejovice, Czech Republic

Crystallization of macromolecular complexes such as dimeric core complex of Photosystem II (OEC PSII) from *Pisum sativum* is influenced by many parameters: purity of sample, homogeneity, capability to form crystals, etc. Tendency to produce suitable crystals for diffraction measurement can be optimized by combination of using different crystallization techniques and other physicochemical parameters (precipitants, additives, pH, etc.) influencing crystallization [1, 2].

Using counter-diffusion method and common vapor diffusion techniques we have tested the influence of several salt additives from Hampton Research screening test (Fe, Ca, Ba, Mg, Ca, Mn, Cd, Cu, Co, Cs, Zn, Y, Ni and Sr), detergents (-DM, $C_{12}E_8$), buffers with different pH (MES, HEPES, Tris, KH_2PO_4, pH 6.0-8.0), and cryoprotectants (PEG with several molecular weight, glycerol, MPD) to find suitable conditions to produce single crystals of diffraction quality. Crystals of hexagonal shape and needles obtained from different conditions will be measured at the synchrotrons DESY, Hamburg (Germany) or ESRF, Grenoble (France).

For computational part of our work interaction energies were calculated by two ways, the point dipole [4] and also point monopole [5] method. The values of interaction energies between transition monopoles, obtained by the point monopole method are generally more precise. Modification of individual transition energies of pigments by so-called electrochromic shifts caused by reduced pheophytin of the D1 branch (Pheo-D1) gave us realistic light-adapted absorption spectra of PSII RC.

We have obtained the temperature dependence of the light-induced difference spectrum under primary acceptor reduction. Almost identical differences in intensities of 298K and 77K-calculated and 277K and 77K-experimental difference absorption spectra clearly supported earlier assumptions [3]. If the molecule of Pheo-D1 is a part of the multimer interaction, its reduction would lead to a change in the exciton interaction and consequently to a change in the optical absorption spectrum. Since the process of exciton interaction is not dependent on temperature and the Pheo-D1reduction does not cause any change in the low temperature CD spectrum, we suppose that the Pheo-D1 molecule is not coupled in the multimer.

1. K.N. Ferreira, T.M. Iverson, K. Maghlaoui, J. Barber, S. Iwata: *Science*, **303** (2004) 1831-1838.
2. I. Kuta Smatanova, J.A. Gavira, P. Rezacova, F. Vacha, J.M. Garcia-Ruiz: *Acta Cryst*., **A61** (2005) 147.
3. F. Vácha, J. Pšenčík, M. Kutý, M. Durchan and P. Šiffel: *Photosynthesis Research*, 84 (2005) 297.
4. V.I. Prokhorenko, D.B. Steensgaard, A.R. Holzwarth: *Biophysical Journal*, **85** (2003) 3173-3186.
5. J. C. Chang: *Chem. Phys*., **67** (1977) 3901-3909.

This work is supported by grants NSM6007665808 and LC06010 of the Ministry of Education of Czech Republic and Institutional research concept AVOZ60870520 of Academy of Science of Czech Republic.

S10

CRYSTALLIZATION OF THREE MUTANTS DERIVED FROM HALOALKANE DEHALOGENASE DHAA OF *Rhodococcus rhodochrous* NCIMB 13064

Alena Stsiapanava[1], Tana Koudelakova[3], Lucie Grodecka[3], Jiri Damborsky[3], and Ivana Kuta Smatanova[1,2]

[1]*Institute of Physical Biology University of South Bohemia Ceske Budejovice, Zamek 136, 373 33 Nove Hrady, Czech Republic*
[2]*Institute of Systems Biology and Ecology Academy of Science of the Czech Republic, Zamek 136, 373 33 Nove Hrady, Czech Republic*
[3]*Loschmidt Laboratories, Faculty of Science, Masaryk University, Kamenice 5/A4, 62500 Brno, Czech Republic*
stepanova@greentech.cz

Microbial growth on halogenated substrates requires the production of catabolitic enzymes that cleave carbon-halogen bonds. Such enzymes are commonly called dehalogenases [1]. Haloalkane dehalogenases (EC 3.8.1.5) are enzymes that belong to the / -hydrolase fold superfamily [2]. These microbial enzymes catalyze the hydrolysis of haloalkanes to the corresponding alcohol, halide, and a hydrogen ion. From this point of view haloalkane dehalogenases are promising bioremediation and biocatalytic agents [3].

Wild-type DhaA was isolated from bacterium *Rhodococcus rhodochrous* NCIMB 13064 [4]. Derived mutant enzymes DhaA04, DhaA14 and DhaA15 were constructed to reveal importance of product transporting pathways (tunnels) in DhaA for its enzymatic activity. Our project is aimed to produce crystals of haloalkane dehalogenases DhaA04, DhaA14 and DhaA15 purified mutants in efficient quality for diffraction experiments and finally compare results with known structure of wild-type DhaA [3].

Standard vapor diffusion technique has been used for searching and optimization of crystallization conditions. Crystallization experiments have been performed in Hampton Research Linbro and Cryschem plates (Hampton Research, CA, USA) as well as in Emerald BioStructures CombiClover Crystallization Plate (EBS plate, Emerald BioStructures, WA, USA) using commercial crystallization kits such as Crystal Screen Lite and Crystal Screen of Hampton Research, and Clear Strategy Screen 1 of Molecular Dimensions Limited (MDL, Suffolk, UK) and also using home-made solutions.

Crystallization experiments with all enzyme mutants are in the progress.

1. Dick B Janssen, Frens Pries, and Jan R. van der Ploeg: Genetics and biochemistry of dehalogenating enzymes. *Microbiology,* **48** (1994) 163-191.
2. Dick B Janssen: Evolving Haloalkane Dehalogenases. *Current Opinion in Chemical Biology,* **8** (2004) 150-159
3. Janet Newman, Thomas S. Peat, Ruth Richard, Lynn Kan, Paul E. Swanson, Joseph A. Affholter, Ian H. Holmes, John F. Schindler, Clifford J. Unkefer and Thomas C. Terwilliger: Haloalkane Dehalogenases: Structure of a *Rhodococcus* Enzyme. *Biochemistry,* **38** (1999) 16105-16114.
4. Anna N. Kulakova, Michael J. Larkin and Leonid A. Kulakov: The plasmid-located haloalkane dehalogenase gene from *Rhodococcus rhodochrous* NCIMB 13064. *Microbiology,* **143** (1997) 109–115.

This work is supported by the Ministry of Education of the Czech Republic (MSM6007665808 and LC06010) and by the Academy of Sciences of the Czech Republic (AVOZ60870520).

Students 3 - Tuesday, June 19

S11

REAL STRUCTURE DEPTH PROFILE OF SHOT-PEENED SURFACE OF A CORROSION-RESISTANT STEEL

J. Drahokoupil[1,2], N. Ganev[1], M. Čerňanský[2], M. Stranyánek[2,3], R. Čtvrtlík[2,3]

[1]Faculty of Nuclear Sciences and Physical Engineering, Czech Technical University, Trojanova 13,120 00 Praha 2, Czech Republic
[2]Institute of Physics of the ASCR, v.v.i., Na Slovance 2, 182 21 Praha 8, Czech Republic
[3]Joint Laboratory of Optics of Palacky University and Institute of Physics of the ASCR, v.v.i., 17. listopadu 50, 772 07 Olomouc, Czech Republic.
jandrahokoupil@seznam.cz

The main goal of this paper is to characterize surface layers of corrosion-resistant steel affected by shot peening. Several experimental methods were used for investigation of samples prepared by using two different levels of shot peening intensity. X-ray diffraction was applied as a main technique for particle size, microscopic and macroscopic residual stress determination. Combination of X-ray diffraction with electrolytic polishing enables to study the depth profile of aforesaid quantities. Nanoindentation and optical microscopy were also applied on polished cross sections of the samples. It was observed that more intensively shot-peened sample differs from the lesser intensively one mainly in the wide of affected zone, which was ca. 0.4 mm and ca. 0.2 mm respectively. Significant correlation was observed between the depth profiles of macroscopic residual stress and particle size. No change in phase content due to surface treating was found.

The obtained depth profiles of residual stresses are plotted in Fig. 1. The lesser intensively shot-peened sample is marked as *C11*, the more intensively one as *C13*. A micrograph of the cross section prepared from the sample *C11* is shown in Fig.2. Black triangles are residual nanoindentation impressions.

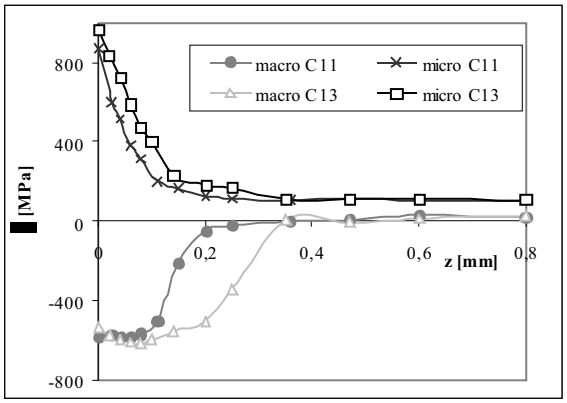

Figure. 1. The depth profile of micro and macro stresses for two intensity of shot-peening – C11 and C13.

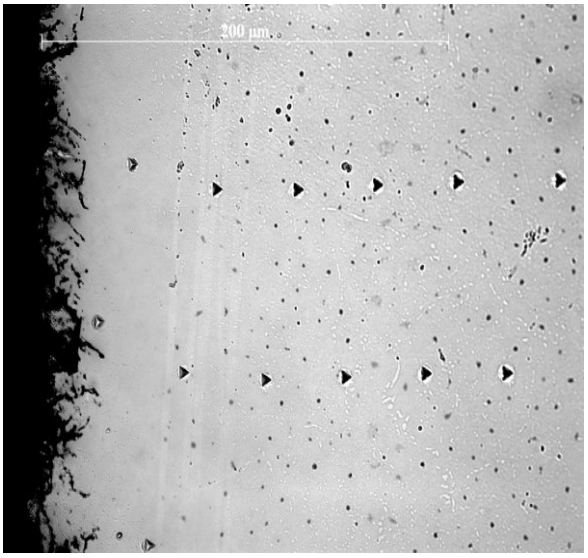

Figure 2. Sample C11, zoom 50x

The research was supported by the Project ą 106/07/0805 of the Czech Science Foundation and by COST 532 action, project No. OC095 and COST 533 action, project No. OC097 of the Ministry of Education, Youth and Sport of the Czech Republic, and by Project MSM 6840770021 of the Ministry of Education, Youth and Sport of the Czech Republic.

Extended contribution submitted for publication in Materials Structure, no. 3.

S12

X-RAY DIFFRACTION STUDY OF DISTRIBUTION OF MACROSCOPIC RESIDUAL STRESSES IN SURFACE LAYERS OF STEELS AFTER GRINDING

Z. Pala[1], N. Ganev[1], J. Jersák[2]

[1]Department of Solid State Engineering, Faculty of Nuclear Sciences and Physical Engineering, Czech Technical University in Prague, Trojanova 13, 120 00 Prague 2
[2]Department of Machining and Assembly, Faculty of Mechanical Engineering, Technical University in Liberec, Hálkova 6, 461 17 Liberec 1
zdenekpala@seznam.cz

The focus of this contribution is analysis of the state of residual stress in surface layers of ground bearing steel (ČSN41 4220) and stainless steel (ČSN41 7135). The influence of various coolants on macroscopic residual stress was investigated. Three forms of cooling were applied: dry grinding, liquid coolant and flow of cold air from a Ranque-Hilsch vortex tube. The surfaces of the samples were analysed by X-ray diffraction technique in six azimuths in order to acquire complete strain tensors. Since 2 -vs.-$\sin^2$ dependences in grinding direction are non-linear and exhibit psi splitting, the method proposed by Dölle and Hauk [1] was used to evaluate tensors of anisotropic trialxial state of residual stress.

The effective penetration depth of CrKá X-ray radiation into ferrous materials for $\sin^2$ = 0,4 is approximately 4 m and therefore removal of surface layers is a necessity in order to pinpoint the distribution of residual stresses beneath the surface. The impact of material removal should cause minimal or neglecting mechanical and thermal distortions to the investigated state of stress. Electro-chemical polishing, which was used, is acknowledged as the most appropriate tool [2].
See page 78 for full paper.

S13

NEW NEUTRON POWDER DIFFRACTOMETER IN NPI ŘEž.

A. V. Chichev

Nuclear Physics Institute of ASCR, CZ - 250 68 Řež, Czech Republic
chichev@ujf.cas.cz

The new neutron powder diffractometer has been designed as a rather universal experimental tool for investigation of crystal and magnetic structures, phase transitions and textures in wide temperature range and/or upon external mechanical loading.

The Monte Carlo simulation software RESTRAX was used for its construction design and optimization. The diffractometer is supposed to operate at constant take-off angle of 70 deg, medium resolution of about $5*10^{-3}$ (d/d) and several wavelengths: 2.074 Å (Cu200), 2.208 Å (Si220), 1.272 Å (Si422).

The instrument is being installed at the 6th neutron horizontal channel of the LVR-15 research reactor in Řež. The diffractometer is equipped with three monochromators easily exchangeable according to the experimental requirements. The He^3 multidetector system is supposed to collect neutron powder diffraction spectra with good resolution in a reasonably short time. The facility will be equipped with a variety of sample environments, such as a furnace, close cycle cryostat, texture goniometer, and deformation testing machine.

S14

IN SITU NEUTRON DIFFRACTION STUDIES OF THE MICROSTRUCTURE RESPONSE OF THE PLAIN FERRITIC STEEL ON TENSILE STRAINING

V. Davydov[1,2]

[1]Nuclear Physics Institute, 250 68 Řež, Czech Republic
[2]Faculty of Nuclear Sciences and Physical Engineering, Czech Technical University in Prague, Břehová 7, 115 19 Prague, Czech Republic

Present neutron diffraction study is aimed on investigation of the response of selected lattice plains in the polycrystalline material in situ upon tensile loading. For this purpose, the 0.1C-0.4Mn construction steel was selected as a simple model material. The tensile deformation test was performed in the incremental mode in which each individual deformation step was followed by unloading. The neutron diffraction spectra were collected both upon loading and unloading and behavior of the diffraction profiles in elastic as well as in plastic region of the deformation curve was examined in detail.

Whereas the behavior of the lattice strains during straining and evolution of the residual intergranular strains (stress type I) have been already described in other papers, the present work focused mainly on profile broadening effects measured in the same deformation regime. The estimate of microstress (root mean square stress) evolution was done by using the single-line profile analysis method. Comparison of microstress values in loaded/unloaded state and in elastic and plastic region offers interesting possibility to separate the contribution of the type II and type III microstresses.

The modification of the TMF [1] method developed for evaluation of the single-line diffraction profiles from high-resolution neutron powder diffractometers is proposed. More sophisticated real space model [2] is used for the distortion and crystallite size broadening of the diffraction lines.

1. P. Strunz, P. Lukas, D. Neov, *J. of Neutr. Res.,* **9** (2001) 99-106.
2. G. Ribarik, T. Ungar, J. Gubicza, *J. Appl. Cryst.,* **34** (2001) 669-676.

This work is supported by the Ministry of Education of Czech Republic (MSMT 2486 G1).

S15

MICROSTRUCTURAL STUDIES OF MATERIALS PREPARED BY SEVERE PLASTIC DEFORMATION

V. Cherkaska[1], R. Kužel[1], Z. Matěj[1], M. Janeček[2], J. Čížek[3], M. Dopita[1,4]

[1]Department of Condensed Matter Physics, [2]Department of Physics of Materials, [3]Department of Low Temperature Physics, Faculty of Mathematics and Physics, Charles University in Prague, Ke Karlovu 5, 121 16 Praha 2, Czech Republic
[4]TU Bergakademie Freiberg, Institute of Materials Science, Gustav Zeuner Str 5, D-09599 Freiberg, Germany

Severe plastic deformation (SPD) is an effective tool for production of compact sub-microcrystalline (SMC), materials of high purity and no residual porosity. In principle, there are two basic techniques – equal channel angular pressing (ECAP) and high-pressure torsion (HPT) [e.g. 1]. In present work, samples prepared by both techniques were studied. Selected samples were pure copper and copper with additions of different amounts of Al_2O_3 and Zr, respectively. The composites are prepared in order to stabilize the fine microstructure to higher temperatures since recrystallization temperature of pure copper is rather low.

The samples were studied by X-ray powder diffraction (PXRD), transmission electron microscopy (TEM), positron life-time spectroscopy and electron back-scattered diffraction (EBSD). Conventional powder diffraction was performed mainly with the aid of Seifert-FPM diffractometer XRD7 and also with Panalytical system X'Pert Pro by using variable divergence slits for keeping the irradiated area fixed and enhancement of high-angle diffraction peaks. The evaluation consisted mainly in the line profile analysis for the estimation of dislocation density and crystallite size. In addition, complete texture measurement was done with Panalytical MRD diffractometer equipped with the Eulerian cradle and polycapillary in the primary beam.

Line broadening analysis showed that the HPT samples (6 GPa, 7 rotations) have smaller crystallite size compare to the ECAP samples, the dislocation densities are similar – of the order of 1×10^{15} m^{-2}. There are only small changes in the mean dislocation density with the increasing number of passes for ECAP (Fig. 1). This fact is well confirmed also by positron annihilation. However, the changes are visible in TEM pictures. After the first pass, the dislocation cells strongly elongated along {111} planes can be seen. Their

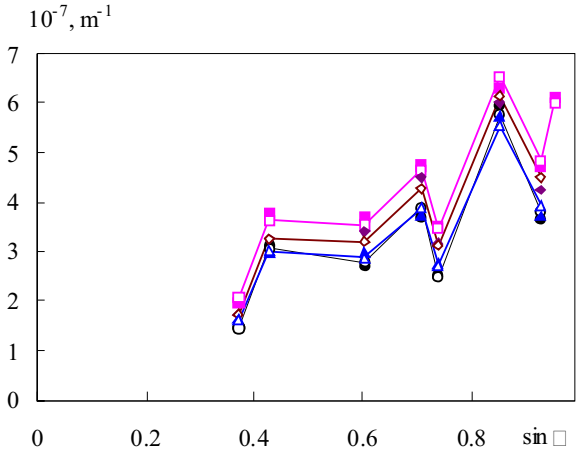

Figure 1. WH plots for the measured transversal direction of Cu samples, prepared with different number of ECAP passes: ●, ○ – 1 pass; ■, □ – 2 passes; ◆, ◇ – 4 passes; ▲, △ – 8 passes showing good agreement of experimental (full symbols) and calculated (empty symbols) data. The calculated data are obtained by assuming common dislocation model for f.c.c. structures.

average size is about 350 nm. Grain boundaries are mainly low-angle. After the second pass the microstructure is not much changed but the grain size is slightly reduced. After the fourth pass, the fraction of equiaxed subgrains increased and the larger proportion of high angle grain boundaries was observed. Equiaxed grain structure was found in about 50 % of the observed area. This is and indication that many new slip systems which are not parallel to the original slip system became active. After eight passes almost homogeneous microstructure with equiaxed subgrains separated by mostly high-angle grain boundaries was observed.

Pole figures obtained from HPT and ECAP are clearly different. The HPT samples usually don't have very strong textures. They are always of fiber type. In several samples two components - (111) and (100) were found. ECAP samples have quite complicated textures that are changing with number and type of passes. The measurements were performed in the plane transversal to the direction of pressing. For one pass, they are in very good agreement with the measurements and simulation in [2]. The dominant component is (111) slightly inclined to the surface. With increasing number of passes more components appear and they are broader. After 8 passes, the (110) component is the strongest one. It seems that in samples with zirconium the texture components are a little sharper.

The above findings were more or less confirmed by the EBSD analysis (Fig. 2). The analysis of the deformed and recrystallized parts indicate changes from deformed part after one pass to about 70% recrystallized fraction after four and eight passes. These changes are not well visible in XRD profiles since the crystallite size in the range above 200 nm is already on the limit of sensitivity of the conventional powder diffraction..

1. R. Z. Valiev, I. V. Alexandrov, R. K. Islamgaliev. Processing and properties of nanostructured materials prepared by severe plastic deformation. Nanostruct. Mater.: Sci. Technol. ed. Chow G.M., Noskova N.I. – NATO ASI: Kluwer Publication. – 1998. – P. 121-143.

2. S. Lia, I. J. Beyerleinb, M.A.M. Bourke, Mat. Sci. Eng. A394 (2005) 66-77.

The work is a part of the research program MSM 0021620834 and also partially supported by the Czech Academy of Sciences under the number KAN400720701.

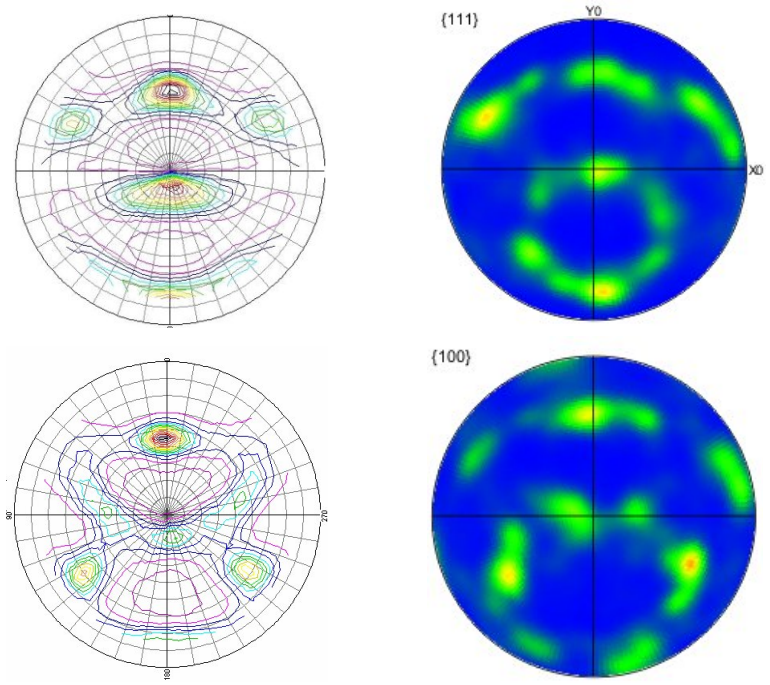

Figure 2. Comparison of pole figures obtained (111) - top and (100) - bottom by XRD (left column) and EBSD (right column) for Cu processed with 1 ECAP pass.

S16

X-RAY DIFFRACTION ANALYSIS OF HEAT-AFFECTED PARTICLES OF TOOL STEEL CH3F12 POWDER

R. Cízlová, M. Kusý

Slovak University of Technology, Faculty of Materials Science and Technology, Institute of Materials Science, J. Bottu 23, 917 24 Trnava, Slovak Republic
romca82@post.sk, martin.kusy@stuba.sk

The investigated tool steel Ch3F12 belongs to the group of tool steels of ledeburte type. This steel is produced by powder metallurgy e.g. rapid solidification (gas atomisation) usually. Powder metallurgy belongs to effective processes of steel production. High quality of products (homogeneous structure, liquation is suppressed) is obtained by PM. At the same time good mechanical, technological and utility properties, which are required from the tool materials, are reached. Materials do not solidify according to equilibrium phase diagram during rapid solidification. It results in final microstructure of elements composed of various metastable phases depending on the size of undercooling and on condition of heat dissipation through the surface of solidifying droplet. As-cast rapidly solidified (RS) particles of Ch3F12 alloy typically consist of metastable austenite and other metastable phases 1 . One of the effects of the rapid solidification is austenite supersaturation with carbon and alloying elements. After rapid solidification and following thermal exposition e.g. (upon the process of compaction or heat treatment) the phase transformation of this austenite occurs and causes a change of materials properties. Therefore, the aim of this analysis was to determine the phase quantity using X-ray diffraction analysis. Analysis revealed the change of the quantity of metastable austenite depending on the temperature of heat-treatment of RS powder particles in comparison with the phase constitution in as-cast state. Furthermore, results show temperature dependence of cell parameters, size of crystallites and crystal strain of RS powder particles.

The experiment comprised of annealing the experimental materials at following temperature 300, 400, 500, 540, 560, 580, 600, 650 and 700 C. The second step was quantitative X-ray diffraction phase analysis, which was performed using program MAUD (Microstructural Analysis Using Diffraction) utilizing the Rietveld method 2 . The change of unit cell parameters, size of crystallites and crystal strain of RS powder particles were evaluated in dependence on the annealing temperature. Mechanical properties of powder particles were revealed with the microhardness measurements.

Analysis showed that thermal exposition of RS particles of Ch3F12 alloy trigger change of the austenite rich in carbon to the ferrite. Simultaneously, the carbide phases are precipitated. This process appears either upon the cooling from the temperature of thermal exposition or at thermal exposition temperature. The transformation from austenite to ferrite was observed to start at 400 C and finish at 560 C. Between 400 C and 500 C the carbide phases was precipitated in the form of the fine precipitates.

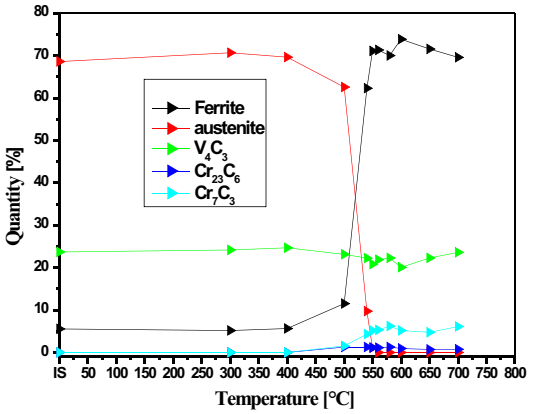

Figure 1. The dependence of phase quantity on the annealing temperature.

Over 500 C the quantity of Cr_7C_3 becomes highest contributing to the maximum microhardness. Above 540 C the phases Cr_7C_3 and $Cr_{23}C_6$ coarsen, therefore the microhardnes decreased. This behavior is also connected together with the fact that from 560 C the sample does not contain longer precipitate hardened austenite 3 . Analysis further showed that transformation from austenite to ferrite is connected with the change of lattice parameters, crystallites and microstrain. Quantities of phases in dependence on the annealing temperature are displayed in Fig.1. The Fig. 2 and 3 shows difference in diffraction patterns and phase quantities. Data in Fig. 2 represents the powder particles in as - cast state where the powder contains 68 vol.% of austenite, 23 vol.% V_4C_3, 6 vol.% ferrite and 3 vol.% of minor phases. Diffraction pattern in Fig. 3 were taken at room temperature from the sample annealed at 540 C, which contained 10 vol.% austenite, 22 vol.% V_4C_3, 62 vol.% ferrite, 4 vol.% Cr_7C_3 and 1,5 % $Cr_{23}C_6$, 0,5 vol.% VN.

The presence of phase transformation from austenite to ferrite was showed to take place during thermal exposition. The kinetics of phase transformation – the austenite changed into the ferrite and precipitates of carbide phases were evaluated using X-ray diffraction analysis. In terms of mechanical properties characterized using microhardness the Ch3F12 tool steel is thermally stabile from 540 C to 600 C 3 . The microhardness decreases sharply above 600 C. It is due to coarsening of the carbide precipitates and ferrite.

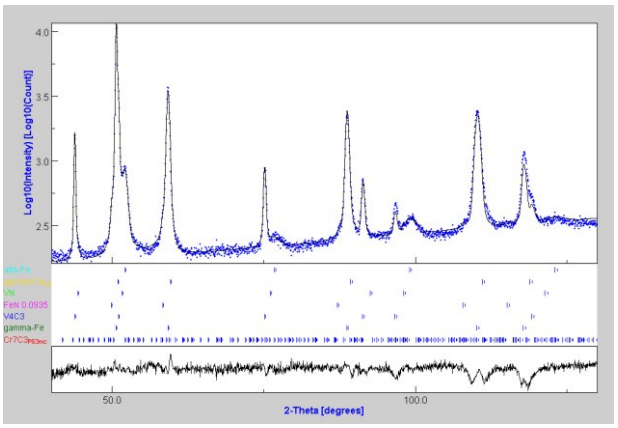

Figure 2. X-ray diffraction pattern of the Ch3F12 powder in as-cast state.

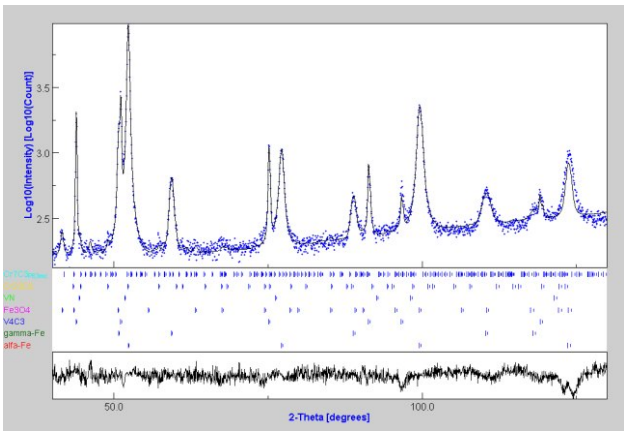

Figure 3. X-ray diffraction pattern of the Ch3F12 powder annealed at 540 °C.

We acknowledge financial support of Slovak Grant Agency VEGA provided to project VEGA 1/4107/07 and VEGA 1/3190/06.

S17

DIFFUSE X-RAY SCATTERING FROM DEFECTS IN Si SINGLE CRYSTALS MEASURED AT VARIOUS TEMPERATURES

V. Valeš[1] and V. Holý[2,1]

[1]Institute of Condensed Matter Physics, Faculty of Science, Masaryk University, Kotlářská 2, CZ – 61137 Brno, Czech Republic,
[2]Department of Condensed Matter Physics, Faculty of Mathematics and Physics, Charles University, Ke Karlovu 5, 121 16 Praha, Czech Republic,
106575@mail.muni.cz

Diffuse x-ray scattering from defects in Czochralski-grown Si wafers (small stacking faults, precipitates of SiO_2, clusters of vacancies or interstitials) is measured at two different temperatures. From the comparison of the reciprocal-space distributions of the intensity scattered at different temperatures we have determined the thermal-diffuse part and the part of the intensity scattered from the structural defects. Since the intensity of thermal diffuse scattering is not affected by the presence of the defects, it can be used as an internal intensity normal. This made it possible to determine reliably the density of structure defects in the wafers.
See page 74 for full paper.

Students 4 - Wednesday, June 20

S18

MAGNETRON DEPOSITED TiO_2 THIN FILMS CRYSTALLIZATION AND TEMPERATURE DEPENDENCE OF MICROSTRUCTURE AND PHASE COMPOSITION

L. Nichtová[1], R. Kužel[1], Z. Matěj[1], J. Šícha[2], J. Musil[2]

[1]Department of Condensed Matter Physics, Faculty of Mathematics and Physics, Charles University in Prague, Ke Karlovu 5, 121 16 Praha 2, Czech Republic
[2]Department of Physics, Faculty of Applied Sciences, University of West Bohemia in Pilsen, Czech Republic

Titanium dioxide (TiO_2) films are nowadays widely used because of their interesting photocatalytic and self cleaning properties. Complex X-ray scattering studies were performed on sets of titanium dioxide thin films sputtered by dual dc magnetron [1]. Several sets of nanocrystalline and amorphous TiO_2 thin films magnetron deposited on glass and silicon substrates have been studied. Phase analysis and X-ray line broadening were studied by X-ray powder diffraction in parallel beam optics; the residual stresses were measured with the aid of the Eulerian cradle and sur-

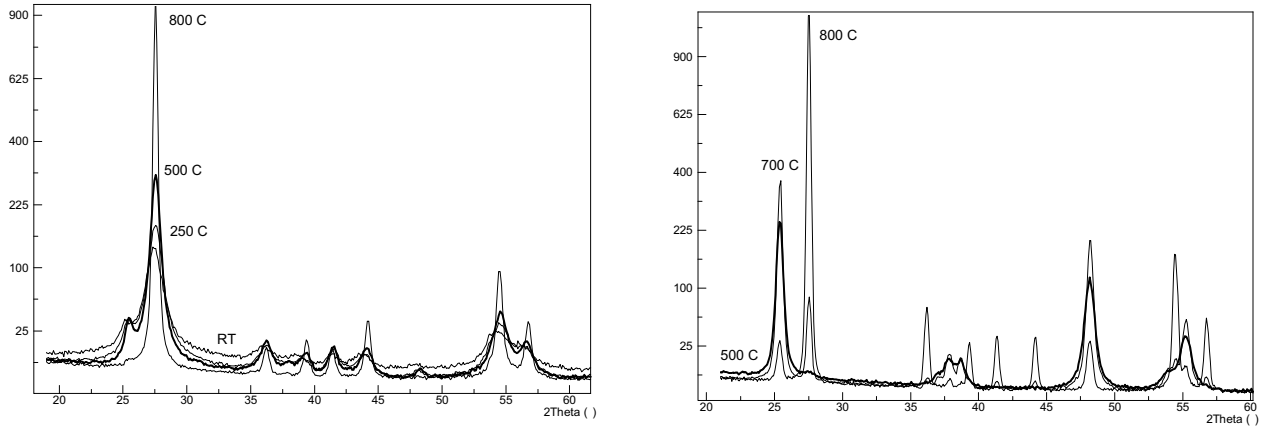

a) b)

Figure 1. Diffraction patterns of TiO_2 films annealed at different temperatures. Strongest peaks of anatase and rutile are 101 at 25° and 110 at 27°, respectively – a) thinner film (220 nm) with dominating rutile and gradually increasing crystallite size with annealing (500 °C, thick line), b) thicker film (935 nm) with dominating anatase after deposition and nearly unchanged crystallite size up to 500 °C (thick line). Anatase is transformed into rutile after annealing at 800 °C. Rutile peaks appeared already after annealing at 700 °C.

face roughness determined by X-ray reflectivity measurement. Microstructure parameters were extracted from XRD measurements by individual peak profile fitting and also by whole powder pattern modelling [2] approach (MAUD [3], modified FOX[4]).

A set of amorphous films with different thickness was studied after annealing and also by in-situ measurements during the heating. It was found that the crystallization temperature started at about 250 °C for thicker films but it was higher for thinner films (< 200 nm) and reached about 350 °C. Thinner films were single phase (anatase) while thicker films above 1200 nm contained also a small amount of nanocrystalline rutile. The crystallite size of these samples immediately after crystallization was larger than 100 nm.

This is clearly different from as-deposited nanocrystalline films. By both thickness dependence of XRD patterns and depth profiling measurements it was found that rutile phase growths on the substrate and it is transformed to anatase with increasing distance from the substrate. This may be caused by temperature gradient during the deposition. Thinner films consist mainly of about 7 nm large rutile crystallites. With annealing temperature the crystallite size is continuously increasing (Figure 1a). By contrast, in thicker films the anatase crystallites of similar size (7 nm) dominate but they remain nearly unchanged with annealing up to 500 °C and then they are transformed to larger rutile crystallites after annealing at 800 °C (Figure 1b).

Simple uniaxial tensile stress and only a weak texture were found for the amorphous films after crystallization. Only for the thinnest films (~ 100 nm), the 101 texture (anatase) was found. In case of nanocrystalline films the stress was low but not uniaxial. This is related to significantly stronger and more complicated texture due to the dual magnetron geometry.

Reflectivity measurements revealed increasing surface roughness with both increasing thickness and annealing temperatures.

1. J. Musil, D. Heřman, J. Šícha (2006). *J. Vac. Sci. Technol.* A24(3), 521-528.
2. P. Scardi, M. Leoni (2002). Acta Cryst. A 58, 190-200.
3. L. Lutterotti, www.ing.unitn.it/~maud.
4. objcryst.sourceforge.net.

The work is a part of the research programs MSM 0021620834 and MSM 4977751302 financed by the Ministry of Education of the Czech Republic and also supported by Grant Agency of the Czech Republic (106/06/0327).

S19

STUDY OF THE STRUCTURE OF GAMNAS THIN LAYERS

L. Horák, V. Holý

Department of Condensed Matter Physics, Faculty of Mathematics and Physics, Charles University, Ke Karlovu 5, 121 16 Prague 2, Czech Republic
Lukas.horak@napismi.cz

In present time there is a big focus on magnetic semiconductors, in which gallium arsenide doped with manganese belongs. It will have a wide application if it is succeeded to raise its Curie temperature to the room temperature. To reach this aim it is necessary to know its inner structure because magnetic properties are connected with positions of manganese atoms in a lattice. According to the theoretical predictions Curie temperature could reach a room temperature for the concentration of manganese ten percents [1].

It results from various studies (e.g. [1]) that a magnetic behavior is caused by added manganese atoms at gallium sites. These atoms act as acceptors and an interaction between their spins is mediated by charge carriers - holes. Donors present in material compensate holes and reduce T_C. Two major problems arise when GaMnAs layer grows. The first problem is a creation of EL2 defect; it means antisites arsenide atoms, which are donors [2]. Their concentration is correlated to the concentration of Mn_{Ga} [1]. The second problem is positioning of Mn atoms, they can occupy not only Ga sites but they can be present as double donor interstitials in As tetrahedrons. Their concentration and influence can be reduced by annealing as described e.g. in [3].

The goal of our work is to obtain a concentration of Mn atoms in substitional and interstitial positions with x-ray diffraction measurement and a concentration of other defects as well. These values should be compared with magnetic measurements to optimize growing layers of desired properties.

We measure rocking curves on different diffractions and we compare them with dynamical calculations of the chosen model. This model comes from GaAs lattice disturbed by added Mn atoms and As antisite defects. It leads to change of lattice constant [4-5] and to local shift of atoms near lattice disturbance changing a structure factor. It is suitable to measure more reflections considering that there are many parameters to fit. Atomic scattering factors of gallium and arsenide differ not too much, so it is useful to measure quazi-forbidden reflections, because change of structure factor due to the defects is the biggest.

Our measured samples are tens nanometers thin layers of GaMnAs containing approximately 5% Mn deposited on low-temperature GaAs buffer on GaAs substrate. Direction [001] is perpendicular to surface. Measurement are done with laboratory difractometer for monocrystals, asymmetric diffractions are measured in coplanar grazing-exit geometry.

I compared measured data with their simulations and there is shown difference of kinematical and dynamical approach in my presentation too. GaMnAs layer is thin enough to use kinematical formulas as described in [6], but there are so many parameters such as shifts of atoms, which make conclusions from kinematical calculations very problematical.

The work is a part of the research program MSM 0021620834 and also partially supported by the Czech Academy of Sciences under the number KAN400720701.

1. T. Junwirth, K.Y. Wang, J. Mašek, K.W. Edmonds, J. König, J. Sinova, M. Polini, N.A. Goncharuk, A.H. MacDonald, M. Sawicki, A.W. Rushforth, R.P. Campion, L.X. Zhao, C.T. Foxon, and B.L. Gallagher, *Phys. Rev. B* **72**, 165204 (2005).
2. M. Kaminska, *Physica Scripta.* Vol. T19, 551-557, 1987.
3. K.W. Edmonds, P.Boguslawski, K.Y. Wang, R.P. Campion, S.N. Novikov, N.R.S. Farley, B.L. Gallagher, C.T. Foxon, M. Sawicki, T. Dietl, M.B. Nardelli, and J. Bernholc, *Phys. Rev. Let.* **92**, 037201.
4. J. Mašek, J. Kudrnovský, and F. Máca, *Phys. Rev. B* **67**, 153203.
5. J. Mašek and F. Máca, *Acta Phys. Polonica A*, **108**, No. 5.
6. G. Kowalski, I. Frymark, and M. Kaminska, *J. Phys. D: Appl. Phys.* **36** (2003) A162-A165.

S20

STANDING-WAVE EFFECTS IN GRAZING-INCIDENCE X-RAY DIFFRACTION FROM POLYCRYSTALLINE MULTILAYERS

J. Krčmář[1], V. Holý[2,1], L. Horák[2], T. H. Metzger[3], and J. Sobota[4]

[1]Institute of Condensed Matter Physics, Masaryk University, Koltářská 2, 611 37 Brno, Czech Republic
[2]Department of Physics of Electronic Structures, Charles University, Ke Karlovu 5, 121 16 Prague, Czech Republic
[3]European Synchrotron Radiation Facility, BP 220, 38043 Grenoble, France
[4]Institute of Scientific Instruments v.v.i., Academy of Sciences of the Czech Republic, Královopolská 147, 612 64 Brno, Czech Republic

In a non-coplanar grazing-incidence geometry of diffraction from a polycrystalline periodic multilayer, the diffracted intensity is modulated by a standing wave created by the interference of the radiation transmitted through the multilayer stack with the wave field specularly reflected from the superlattice interfaces. Similarly, the radiation being diffracted from the polycrystalline structure is reflected specularly from the interfaces and a standing-wave interference pattern results as well. This paper shows a series of experimental measurements obtained from C/Ni periodic multilayers demonstrating this effect. The experimental data have been modeled using a theoretical approach based on the distorted-wave Born approximation. The method can be used for a study of the profiles of the grain sizes and strains across the multilayer.

Extended contribution submitted for publication in Materials Structure, no. 3.

S21

KINETIC MONTE CARLO SIMULATION OF QUANTUM-DOT NUCLEATION IN PbSe/PbEuTe MULTILAYERS

M. Mixa[1], V. Holy[1], G. Springholz[2], D. Lugovyy[2]

[1]Department of Condensed Matter Physics, Faculty of Mathematics and Physics, Charles University, Ke Karlovu 5, 121 16 Praha, Czech Republic
[2]Institute of Semiconductor Physics, Johannes Kepler University, Altenbergerstr. 69, A-4040 Linz, Austria
martin.mixa@centrum.cz

PbSe/PbEuTe quantum-dot multilayer is an interesting example of a self-organized semiconductor nanostructure. In this system the self-assembly phenomenon is caused by the elastic deformation of crystal lattice due to the lattice mismatch between both materials. Depending on the thickness of the PbEuTe spacer layer, three different arrangements of the PbSe dot superlattice are experimentaly observed (vertical and trigonal arrangements of the dots as well as non-correlated mode of dot positions).

In our theoretical study of the epitaxial growth and the self-organization processes in this system we use the kinetic Monte Carlo method for the simulation of the PbSe dot nucleation. The nucleation probability of a quantum dot at the surface of a particular PbSe layer is influenced by the local chemical potential of migrating adatoms and consequently by the local surface elastic energy induced by the dots on the PbSe/PbEuTe interfaces buried below the surface. This energy distribution is taken into account for the movement simulation of atoms deposited on the growing surface. Changing the spacer layer thickness we obtain the same dot-superlattice arrangements as in the experiments.

This work is a part of the research plan MSM 0021620834 that is financed by the Ministry of Education of the Czech Republic. The work was also supported by the Grant Agency of Academy of Sciences of the Czech Republic (project KAN400100652).

Students 5 - Thursday, June 18

S22

SYNTHESIS OF -Fe AND Fe_2Zr PARTICLES EMBEDDED IN ZrO_2 MATRIX

P. Roupcová, O. Schneeweiss

Ústav fyziky materiálů AV ČR v.v.i., Žižkova 22, 616 62 Brno
roupcova@ipm.cz

Iron and Fe_2Zr nanoparticles in zirconium oxide matrix have been prepared by heat treatment of a mixture of ferrihydrite and zirconium hydride powders. Changes in the phase composition of the as-mixed powders during annealing in vacuum at 620 °C and 800 °C were monitored using measurement of thermomagnetic curves and XRD in heating chamber. Structure and phase composition of the final products were characterized by X-ray powder diffraction and ^{57}Fe Mössbauer spectroscopy. The influence of the composition of the original mixture and temperature on the final properties of the composites are discussed. The XRD determined 55 % monoclinic ZrO_2, 23 % Fe_2Zr, 14 % Zr and 8 % -Fe phases in the sample annealed at 800 °C. The mean coherent length was 20-80 nm. The annealing at 620 °C does not create the Fe_2Zr and the sample consists of 39 % monoclinic ZrO_2, 35 % Zr, 22 % -Fe and 4 % ZrH_2 phases.
See page 85 for full paper.

S23

PREPARATION AND STRUCTURE OF TITANATE NANOTUBES

D. Králová [1], E. Pavlova [1], M. Šlouf [1,2], R. Kužel [3]

[1]Institute of Macromolecular Chemistry, Academy of Sciences of the Czech Republic, Heyrovskeho nam. 2, 162 06 Praha 6, Czech Republic
[2]Member of Consortium for Research of Nanostructured and Crosslinked Polymeric Materials (CRNCPM)
[3]Department of Electronic Structures, Faculty of Mathematics and Physics, Charles University, 121 16 Praha 2, Ke Karlovu 5, Czech Republic
kralova@imc.cas.cz

This work describes simple and reproducible preparation of dried and stable titanate nanotubes (Ti-NT) in gram-scale amounts using freeze drying. Ti-NT represent a novel type of nanoparticles with interesting morphology and peculiar structure. The morphology, crystalline structure and elemental composition of Ti-NT were investigated by means of scanning and transmission electron microscopy, X-ray and electron diffraction and X-ray diffraction.

Extended contribution submitted for publication in Materials Structure, no. 3.

S24

SYNTHESIS AN STRUCTURE OF CoGeTe AND $CoSn_{1.5}Te_{1.5}$

F. Laufek[1], J. Navrátil[2], M. Plášil[3]

[1]Czech Geological Survey, Geologická 6, Praha 5, 152 00, Czech Republic
[2]Joint Laboratory of Solid State Chemistry of IMC AS ČR and University of Pardubice, Studentská 84, 532 10 Pardubice, Czech Republic
[3]Charles University, Faculty of Science, Albertov 6, Praha 2, 128 43, Czech Republic
laufek@cgu.cz

This presentation is a part of systematic investigations on crystal structures and physical properties of M-X-Ch compounds of cobalt-group metals (M = Co, Ir, Rh) and main group IV and VI elements (X = Si, Ge, Sn; Ch = S, Se, Te). These phases are of interest in materials science because of their possible thermoelectric applications.

The ternary compounds, CoGeTe and $CoSn_{1.5}Te_{1.5}$ were synthesised from the elements by high temperature solid state reactions. Co powder was at first heated at

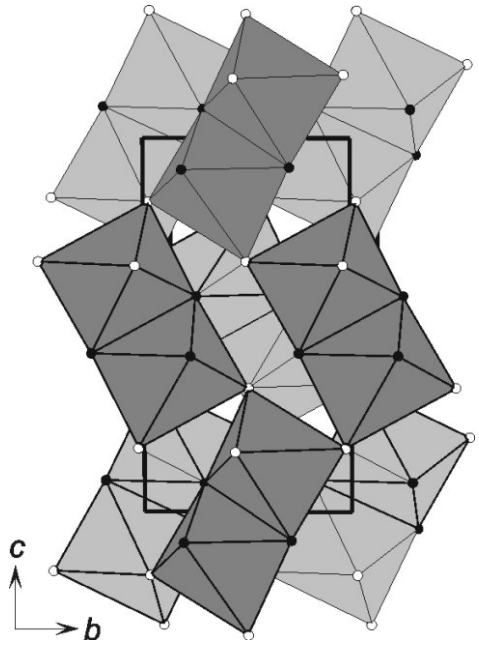

Figure 1. Polyhedral representation of CoGeTe structure showing the [$CoGe_3Te_3$] octahedra. Black and white circles are Ge and Te atoms, respectively.

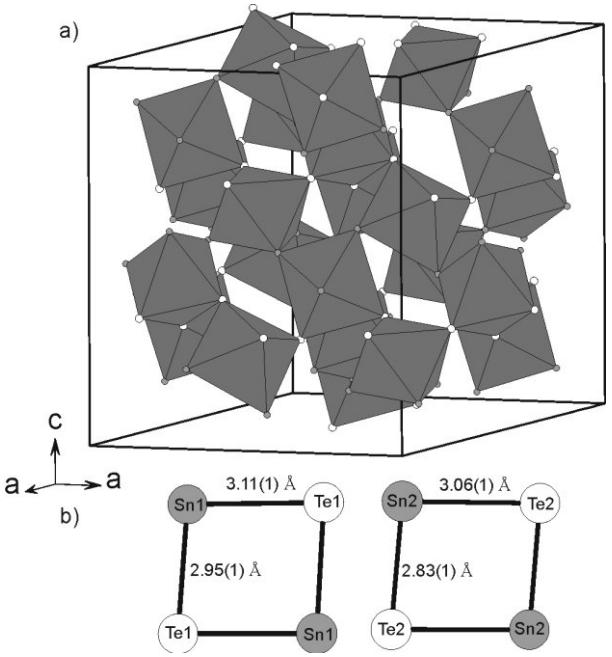

Figure 2. (a) Polyhedral representation of $CoSn_{1.5}Te_{1.5}$ structure showing the corner sharing arrangement of the [$CoSn_3Te_3$] octahedra. (b) Four-member Sn_2Te_2 rings .

800 °C for 1 hr in H_2 atmosphere to remove possible oxides. Stoichiometric amounts of Co (99.99%), Ge (99.99%), Sn (99.99 %) and Te (99.99%) were sealed in evacuated quartz tubes and heated at 1150 °C for 4 hrs. Following this, the samples were ground using the agate mortar and pestle, and sealed again under vacuum in quartz tubes. The mixtures were heated at 550 °C for three days. The resultant material was once again ground and heated at 670 °C and 600 °C for CoGeTe and $CoSn_{1.5}Te_{1.5}$, respectively. After long-term annealing, the samples were quenched in cold water.

Here we report a detailed structural study on the two ternary compounds CoGeTe and $CoSn_{1.5}Te_{1.5}$. As single crystals of sufficient quality were not available, the analyses were performed on powder samples. The crystal structure of CoGeTe was solved by direct methods by means of EXPO2004 [1] program package, while the inicial structure model for $CoSn_{1.5}Te_{1.5}$ was derived from data published for $CoGe_{1.5}Te_{1.5}$ [2]. Both structures were refined by Rietveld method by means of FullProf program [3].

CoGeTe: space group *Pbca*, a = 6.1892(4), b = 6.2285(4), c = 11.1240(6) Å, Z = 8, R_{wp} = 0.083, R_B = 0.065. The crystal structure of CoGeTe can be viewed as a ternary ordered variant of -$NiAs_2$ (also known as a mineral pararammelsbergite), which is transitional between the marcasite-type and the pyrite-type structures. Each Co atom is surrounded by three Ge and Te atoms showing a distorted octahedral coordination. One octahedral edge is shared with an adjacent octahedron, compared to two shared edges in the marcasite structure and none in the pyrite structure. Other vertices of the [$CoGe_3Te_3$] octahedron are connected by corners sharing. (Fig. 1). Similar description has been described for PtSiSb [4].

$CoSn_{1.5}Te_{1.5}$: space group R-3, a = 12.9062(2), c = 15.7837(3) Å, Z = 12, R_{wp} = 0.106, R_B = 0.046. The structure of $CoSn_{1.5}Te_{1.5}$ can be described as a modification of a cubic structure of $CoSb_3$ [5] (skutterudite type). The weak superstructure reflections found in powder diffraction pattern reveal the ordering between Sn and Te atoms. This ordering reduces the symmetry from cubic to rhombohedral. Each Co atom is surrounded by three Te and Sn atoms forming a distorted octahedral coordination. The [$CoSn_3Te_3$] octahedra share only corners with six neighbouring octahedra. One of the most characteristic features of the $CoSn_{1.5}Te_{1.5}$ structure is the presence of two distinct four-member rings [Sn_2Te_2] (Fig 2). The schematic representation of the $CoSn_{1.5}Te_{1.5}$ structure is shown in the Fig. 2. A compound with this composition was mentioned at the conferences [6, 7] but no structural details were given.

1. A. Altomare, R. Caliandro, M. Camalli, C. Cuocci, C. Giacovazzo, A. Moliterni. R. Rizzi, *J. Appl. Cryst*., **37,** (2004), 1025.

2. P. Vaqueiro, G.S. Sobany, A.V. Powell, K.S. Knight, *J. Solid State* Chem., **179,** (2006), 2055.

3. J. Rodríguez-Carvajal, *FullProf.2k*, Laboratoire Léon Brillouin, France, 2006.

4. M. Wang, M.G. Morgan, A. Mar, *J. Solid State Chem*., **175**, (2003), 231.

5. Th. Schmidt, G. Kliche, H. D. Lutz, *Acta Crystallogr*.. **C 43**, (1987), 1978.

6. Y. Nagamoto, K. Tanaka, T. Koyanagi, Proceeddings of the 16th International Conference on Thermoelectrics, Dresden, Germany.

7. A. Smaleez, Q. Lin, D. C. Johnson, J. Mertin, Material Research Meeting 2005, p. 137., Boston, USA.

This study was supported by the Grant Agency of the Academy of Sciences of the Czech Republic (Project No. KJB 300130612), by the internal project of the Czech Geologi-

cal Survey (Project No. 3230) and by the Czech Science Foundation (Project No. 203/07/0267).

S25

SOLID-STATE SYNTHESIS, CHARACTERIZATION AND APPLICATIONS OF POTASSIUM FERRATE(VI): A MULTI-ANALYTICAL APPROACH

J. Filip[1], L. Machala[1], R. Zbořil[1], V. K. Sharma[2], I. Medřík[1]

[1]Centre for nanomaterial research, Palacký University Olomouc, Svobody 26, 771 46 Olomouc, Czech Republic
[2]Chemistry department, Florida Institute of Technology, 150 West University Boulevard, Melbourne, FL 32901, USA
jan.filip@upol.cz

In the recent years, there has been increasing interest in the +6 oxidation state of iron. The ferrate(VI) ion ($Fe^{VI}O_4^{2-}$) is the only one known species [1], important because of its potential use in high energy density rechargeable batteries, in "greener" technology for organic synthesis, and in treatment of contaminants and toxins in water and wastewater [2]. Potassium ferrate(VI) (K_2FeO_4) is the most studied compound among the family of ferrate(VI) [2]. Hence, solid orthorhombic, few micrometer-sized crystals of potassium ferrate(VI) were synthesized by thermally induced solid-state reaction, where KNO_3 and suitable iron-containing compounds (mostly cheap waste iron oxides, oxyhydroxides and sulfates, available in high quantities) were heated together to obtain K_2FeO_4. However, the im-

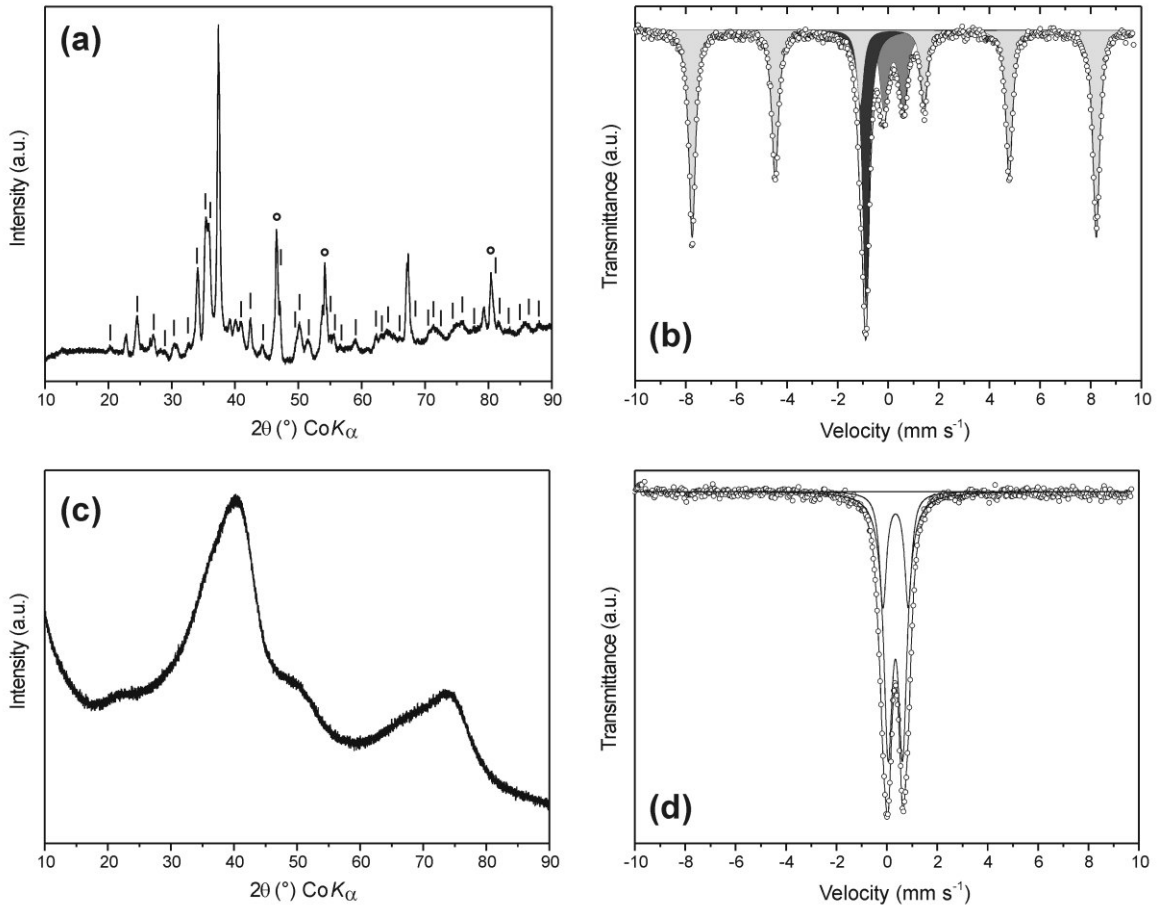

Figure 1. (a) X-ray powder diffraction pattern of synthesized mixture of K_2FeO_4 and $KFeO_2$, vertical lines indicate X-ray diffraction peaks of K_2FeO_4, circles mark the Pt-holder as the pattern was measured under vacuum to protect the sample reaction with air moisture during the experiment; (b) ^{57}Fe Mössbauer spectrum of synthesized mixture of K_2FeO_4 and $KFeO_2$, dark gray – subspectrum corresponding to K_2FeO_4, light gray - $KFeO_2$, medium gray – amorphous iron oxyhydroxides; (c) X-ray powder diffraction pattern and (d) ^{57}Fe Mössbauer spectrum of two-line ferrihydrite forming during the reaction of K_2FeO_4 with pollutants in aqueous solution.

mediate decomposition of ferrate(VI) occurs at elevated temperatures used in a thermal synthesis technique [3], which results in a low yield of K_2FeO_4 product. An increase in the K_2FeO_4 yield was achieved by optimizing the precursor composition and the temperature conditions under which the secondary decomposition is reduced. ^{57}Fe Mössbauer spectroscopy and X-ray powder diffraction analyses were routinely used to monitor the process of synthesis.

Resulting potassium ferrate(VI) (space group *Pnam*) reveals the refined lattice parameters, a = 7.702(2), b = 10.346(1), c = 5.862(1) Å, and cell volume 467.1(1) Å^3, which are close to those reported by other researchers. Potassium ferrate(VI), or mixture of potassium ferrate(VI) and potassium iron(III) oxide ($KFeO_2$) (Fig. 1a,b), depending on the procedure used, was found to be very effective in technology of water treatment under laboratory conditions [2, 4]. In all cases, the final reaction product of potassium ferrate(VI) decomposition and Fe^{6+}–to–Fe^{3+} reduction is two- to six-line ferrihydrite ($Fe_5HO_8{\cdot}4H_2O$) (Fig. 1c,d) of large surface area and nanocrystalline character (the mean particle size of ferrihydrite calculated from broadening of diffraction peaks according to the Scherrer formula and confirmed by transmission electron microscope equals to mean 5 nm), or mixture of ferrihydrite with better crystalline phases (e.g., goethite), depending on the type of pollutants and reaction kinetics. Just the nanocrystalline character and large surface area (up to 183 m^2/g measured using a Brunauer-Emmett-Teller – BET – surface area analyzer) of final iron oxyhydroxides is a unique phenomenon, great for a possible usage of potassium ferrate(VI) in water treatment technologies. Hence, the initially oxidized toxic metals and other pollutants are effectively adsorbed on and/or co-precipitated with the subsequently formed iron oxyhydroxides.

^{57}Fe Mössbauer spectroscopy (room- and low-temperature, and in-field configuration), together with X-ray powder diffraction, represent powerful tools in monitoring the phase composition and structural properties of the synthesized potassium iron(III, VI) oxides, their stability and reaction mechanisms with pollutants. Mössbauer spectroscopy gives a unique information about the oxidation state of iron, phase composition and phase ratio of iron-bearing and even amorphous phases, whereas X-ray powder diffraction brings the possibility to add both qualitative and quantitative data to all presented, mainly crystalline phases. The presented results have a practical impact for the optimization of the solid-state synthesis of potassium ferrate(VI). Moreover, new data will be presented in terms of phase composition of reaction products of potassium ferrate(VI), as well as potassium iron(III) oxide and their mutual mixture.

1. J. F. Berry, E. Bill, E. Bothe, S. D. George, B. Mienert, F. Neese, K. Wieghardt, *Science*, **312**, (2006), 1937-1941.
2. V. K. Sharma, *Adv. Environ. Res*, **6**, (2002), 143-156.
3. L. Machala, R. Zbořil, V. K. Sharma, J. Filip, O. Schneeweiss, Z. Homonnay, *J. Phys. Chem B*., **111**, (2007), 4280-4286.
4. V. K. Sharma, F. Kazama, H. Jiangyong, A. K. Ray, *J. Water Health*, **3**, (2005), 45-59.

Financial supports from the Ministry of Education of the Czech Republic (MSM6198959218 and 1M6198959201) and from Academy of Sciences of the Czech Republic (KAN108040651) are gratefully acknowledged.

S26

MOLECULAR MODELLING OF LAYERED DOUBLE HYDROXIDE INTERCALATED WITH BENZOATE

Petr Kovář and Pavla Čapková

Faculty of Mathematics and Physics, Charles University Prague, Ke Karlovu 3, 12116 Prague 2, Czech Republic
kovar@karlov.mff.cuni.cz

The structure of Zn_4Al_2 Layered Double Hydroxide (LDH) intercalated with benzencarboxylate ($C_6H_5COO^-$) was solved by methods of molecular modelling related to diffraction. Molecular modelling using empirical force field was carried out in Cerius^2 modelling environment. A series of starting models with various orientation (parallel, tilted and perpendicular) of guest anions with respect to the host layers was created. According to the comparison of total crystal energy of optimized structure models with different geometry it was found out that benzoate anions are almost perpendicular to LDH layers, anchored to OH groups of the host layers via hydrogen bonds. Mutual orientation of benzoate ring planes in the interlayer space keeps parquet arrangement. Water molecules are roughly arranged in planes adjacent to host layers together with COO^- groups. Calculated basal spacing d_{calc} = 15.2 Å is in good agreement with experimental basal spacing d_{exp} = 15.3 Å.

Extended contribution submitted for publication in Materials Structure, no. 3.

S27

MOLECULAR SIMULATIONS OF HYDROTALCITE INTERCALATED WITH PYRENETETRASULFONATE

Marek Veteška, Miroslav Pospíšil

Charles University, Faculty of Mathematics and Physics, Department of Chemical Physics and Optics, Ke Karlovu 3, 121 16 Prague 2, Czech Republic, veteska@karlov.mff.cuni.cz

In this work hydrotalcite-like structures intercalated by pyrenetetrasulfonate anions were calculated by methods of molecular simulations (i.e. the molecular mechanics and the classical molecular dynamics). The hydrotalcites are layered materials with anions and water molecules which are held between layers only by nonbond interactions. Molecular simulations are based on empirical force fields intended for calculations of optimized structures with minimal potential energy.

Based on experimental data (X-ray diffraction and thermogravimetry) rough initial models were build for 4 different distances between the hydrotalcite layers with 2 pyrenetetrasulfonate anions in the first interlayer. About 4*10 different suitable initial models destined for the molecular mechanics were sequentially selected from roughly 4*12 billion possible models by systematic scanning an entire state space (algorithm Supramol). The experimentally determined amount of water molecules was randomly inserted into relevant models. After various techniques of calculations (molecular mechanics with free cell parameters, using a pressure, various techniques of charge calculation, systematic bending of sulfonates, various initial position of water molecules) it appeared as optimal to calculate with rigid hydrotalcite layers and cell parameters and with charges calculated separately for every molecule and layer. Arrangement of water was refined by subsequent molecular dynamics.

The sample with interlayer distance 9,83 Å *and 0 water molecules.* The resulting energy of models with anions positioned in one layer parallel with hydrotalcite layers or with anions slightly tilted were very similar. It can be assumed that all these calculated models could appear in the real sample or arrangement of molecules in the interlayer is slightly variable.

The sample with interlayer distance 13,63 Å *and 36 water molecules.* The resulting energy of models with anions situated in 2 horizontal layers approximately in the thirds of the interlayer, variously turned, shifted and tilted were very similar, too. Thus arrangement of molecules in the interlayer is again slightly variable. The water molecules form three layers, first one in the middle, two ones in the quarters of the interlayer.

The sample with two interlayer distances 11,74 Å *and 12,81* Å *and 25 water molecules.* On the base of calculations it seems to be the most probable that the measured sample were not stabilized and therefore it appears as two-phase.

This work was supported from Ministry of Education of the Czech Republic MSM 0021620835 and GAČR 203/05/2306.

Extended contribution submitted for publication in Materials Structure, no. 3.